Nonlinear dynamics in periodic phase space

A. Iomin, D. Gangardt, and S. Fishman
Physics Department, Technion, Haifa 32000, Israel
(Received 28 July 1997)

Regular and chaotic dynamics of a system with periodic phase space perturbed by an alternating external field is considered. It is relevant for the electronic motion in two dimensions in the presence of a uniform magnetic field and a perpendicular alternating electric field. The phase space is divided into cells embedded in a chaotic mesh. Bifurcations of resonances within the cells are studied. Transport takes place in the chaotic mesh. It is analyzed in the framework of the separatrix map. Accelerator modes are found for some values of parameters and their bifurcations are investigated. Their effects on transport in phase space are discussed. [S1063-651X(98)04004-5]

PACS number(s): 05.45.+b, 05.60.+w, 05.40.+j

I. INTRODUCTION

The investigation of motion of lattice electrons in the presence of electric and magnetic fields represents an important task in the study of solids, in particular in the study of the Fermi surfaces structure (see, for example, [1,2] and references in these books). In some situations this many-body problem can be reduced to a one-particle problem of motion on the Fermi surface [2,3]. In many situations it is sufficient to investigate this motion in the classical limit. In the present work the *classical* behavior of a model system for an electron gas moving in a constant magnetic field and perpendicular alternating electric field is studied. It exhibits dynamical phenomena that are of interest beyond the original system that motivated this strongly. These phenomena may be important for the understanding of absorption of radiation and transport in these systems.

The motion of an electron on the Fermi surface in the presence of an alternating electric field and a constant magnetic field is an example of nonlinear motion with a possible transition to a chaotic regime [4–6]. The conditions for the validity of classical description are assumed to hold [3]. In [4] the electronic motion in a two-dimensional periodic potential in the presence of a perpendicular magnetic field was studied. In this work it was shown that the appearance of chaotic motion is due to a nonlinear coupling between two degrees of freedom by the magnetic field. It was also shown that nonlinear resonances and chaotic motion of an electron have physical meaning for magnetotransport effect in lateral surface superlattices [5]. The nonstationary system was investigated where the chaotic motion resulted from a nonlinear time-dependent electric field [6]. A detailed study of nonlinear motion taking place in periodic phase space and the main properties of normal diffusion in the phase space due to this periodicity have been reported in [6] as well. Anomalous diffusion properties have been investigated in [7].

In the present work the electronic motion on the Fermi surface is considered. Nonlinear resonant properties of periodic phase space are considered for both an isolated resonance approximation and chaotic motion inside separatrix layers. Two types of bifurcations are studied. The first one is a central elliptic point where the regular dynamics and bifurcate confluence of elliptic and hyperbolic points are considered. It is shown that this bifurcation is due to the frequency change of the perturbation. The second point is an acceleration mode, which is responsible for ballistic motion on a separatrix mesh. The diffusive process inside the separatrix layers is studied. The maximal length of ballistic trajectories contributing to the diffusive process is evaluated as well.

It is assumed in the following consideration that the alternating electric field $\vec{E}$ is spatially homogeneous (i.e., the system size is much smaller than the wavelength) and perpendicular to the direction of the magnetic field $\vec{H}$. In this case the motion is fully described in the Fourier space of reciprocal lattice vectors $\vec{k}$. The components of the mechanical momentum $\hbar\vec{k}$ lying in the plane orthogonal to $\vec{H}$ appear to form a canonical pair. Thus, in the case of the particular choice $\vec{H}=(0,0,H)$ it follows that $\dot{k}_z=0$ and the other two components are canonical conjugated variables [8]

$$\dot{k}_x=-\frac{eH_z}{\hbar c}v_y, \quad \dot{k}_y=\frac{eH_z}{\hbar c}v_x, \quad \vec{v}=\frac{1}{\hbar}\vec{\nabla}_k\varepsilon. \tag{1}$$

The corresponding effective Hamiltonian of one-particle motion is determined by the Fermi surface shape $\varepsilon=\varepsilon(k_x,k_y,k_z)$ and the electric field is considered as a perturbation.

The case of a simple cubic (sc) lattice is considered. Therefore, in the tight-binding approximation the Fermi surface is determined by [8]

$$\varepsilon(\vec{k})=-\alpha-\gamma(\cos k_x a+\cos k_y a+\cos k_z a), \tag{2}$$

where α is the energy of lattice electron, γ is the overlap integral in tight-binding approximation, and a is the lattice constant. The magnetic field is chosen along the z axis: $\vec{H}=H\hat{z}$, while the electric field has the form $\vec{E}=(0,E_0\sin\tilde{\nu}t,0)$. In this case the equations of motion (1) corresponding to the (sc) dispersion law (2) in the presence of the perturbative electric field read

$$\dot{p}=-\sin q-\epsilon\sin\tilde{\nu}t,$$

$$\dot{q}=\sin p. \tag{3}$$

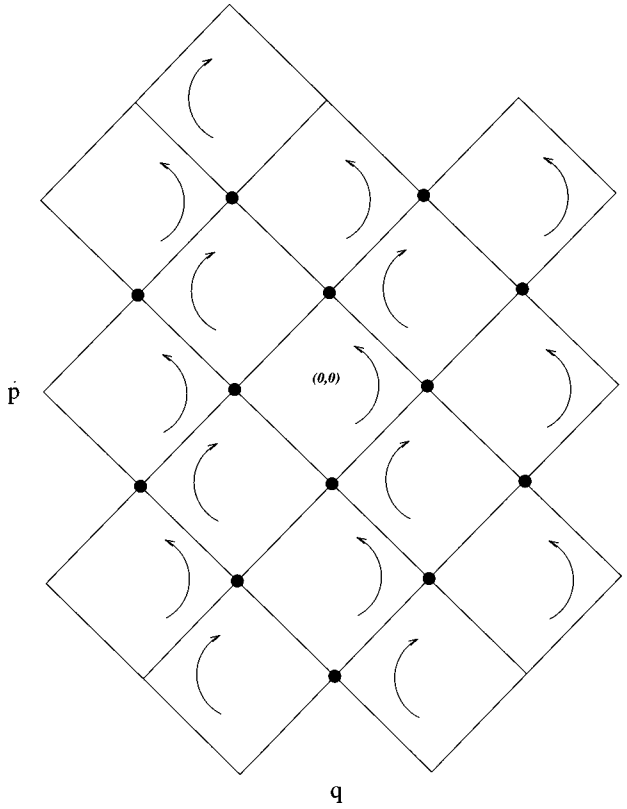

FIG. 1. Separatrix mesh.

Here p,q,t are the dimensionless generalized momentum, coordinate, and time, respectively, defined by relations

$$p=k_y a, \quad q=k_x a, \quad t\to\Omega t,$$

$$\nu=\tilde{\nu}/\Omega, \quad \epsilon=\frac{eE_0 a}{\hbar\Omega}, \tag{4}$$

where $\Omega=eH/cm^*$ is the cyclotron frequency of an electron with effective mass $m^*=\hbar^2/\gamma a^2$. The effective Hamiltonian that generates the equation of motion (3) is of the form

$$\mathcal{H}=-(\cos p+\cos q)+\epsilon q\ \sin\nu t=\mathcal{H}_0(p,q)+\epsilon V(p,q,t). \tag{5}$$

One should note the fact that Eqs. (3) are invariant with respect to the translations

$$p\to p+2n\pi, \quad q\to q+2m\pi \tag{6}$$

as well as

$$p\to p+(2n-1)\pi, \quad q\to q+(2m-1)\pi, \quad t\to -t \tag{7}$$

for integers n and m. The latter case corresponds to the description of holes. Therefore, the phase space is naturally divided into $2\pi\times 2\pi$ cells as shown in Fig. 1.

The effects of a small perturbation ($\epsilon\ll 1$) will be studied in the present work. Such a perturbation is weak enough so that the basic cell structure of phase space is not destroyed. As a result of the perturbation, however, the sharp boundaries between the cells are replaced by the separatrix layer. In Sec. II the effect of the perturbation on the motion deep inside the cell is studied. This results in a bifurcation of classical resonances. In Sec. III the separatrix map that describes the dynamics in the separatrix layer is studied. The resulting motion is usually diffusion in phase space leading to growth of energy that is linear in time. For specific values of the parameters accelerator modes are found, leading to a quadratic increase in energy. These are studied in Sec. IV. The conclusions are summarized in Sec. V.

II. BIFURCATE SHRINKING OF THE PHASE SPACE

The unperturbed Hamiltonian $\mathcal{H}_0$ describes a finite motion with a nonlinear frequency $\omega(\mathcal{H}_0)$ in a cell bounded by a separatrix, defined by the condition

$$\cos p+\cos q=0. \tag{8}$$

The solution corresponding to unperturbed motion with the Hamiltonian $\mathcal{H}_0$ can be found from the equation of motion (3) with $\epsilon=0$. It follows from Eq. (3) that the expression for time reads

$$t=\int_0^q\frac{dq'}{\dot{q}}=\int_0^q\frac{dq'}{\sqrt{1-(\mathcal{H}_0+\cos q')^2}}. \tag{9}$$

After a change of variable $x'=\cos q'$, we obtain

$$t=\int_x^1\frac{dx'}{\sqrt{(1-\mathcal{H}_0-x')(1-x')[x'-(-1-\mathcal{H}_0)][x'-(-1)]}}$$
$$=F(\psi,k), \tag{10}$$

where

$$\psi=\arcsin\sqrt{\frac{2(1-\cos q)}{(2+\mathcal{H}_0)(1-\mathcal{H}_0-\cos q)}},$$

$$k=\sqrt{1-\frac{\mathcal{H}_0^2}{4}}, \quad \mathcal{H}_0<0, \tag{11}$$

and $F(\psi,k)$ is the incomplete elliptic integral of the first kind with a modulus k [9]. The period is $T=4F(\pi/2,k)=4K(k)$ and the corresponding frequency is

$$\omega(k)=\frac{2\pi}{T}=\frac{\pi}{2K(k)}, \tag{12}$$

where $K(k)$ is the complete elliptic integral of the first kind. With the usual notation $\sin\psi=\sin am(F)=$ sn t, one obtains the solution

$$\sin p=2k\sqrt{k'(1+k')}\frac{\mathrm{cn}\ t}{\mathrm{dn}^2 t+k'}, \tag{13}$$

where $k'=\sqrt{1-k^2}$ is the complementary modulus and sn, cn, and dn are the Jacobi elliptic functions with common real period of $4K(k)$. Note that the quantity $\omega_c=\Omega\omega(k)$ is the frequency with corresponding effective cyclotron mass m^* of an electron.

When the external field ϵV is added to the Hamiltonian $\mathcal{H}_0$ in Eq. (5) there appear nonlinear resonances. For the following analysis, carried out in the isolated resonance ap-

proximation [10–12], it is convenient to change to the $[k,\theta=\omega(k)t]$ variables. From Eqs. (3) and (13) one obtains the equations of motion for the (k,θ),

$$\dot{k}=\frac{dk}{d\mathcal{H}_0}\frac{d\mathcal{H}_0}{dt}=\frac{dk}{d\mathcal{H}_0}[\mathcal{H}_0,\mathcal{H}]_{PB}=-\epsilon\left(\frac{dk}{d\mathcal{H}_0}\right)\sin p\ \sin\nu t, \tag{14a}$$

$$\dot{\theta}=\omega(k)+O(\epsilon). \tag{14b}$$

Since in the resonant perturbation theory expansions of order $\sqrt{\epsilon}$ are performed, terms of order ϵ can be neglected in Eq. (14b).

To obtain an expression for the nonlinear resonances, we expand $\sin p$ in the Fourier series over θ. The Fourier expansion of $\sin p$ is (see the Appendix)

$$\sin p=\sum_{m=0}^{\infty}\frac{\omega\cos\left(\frac{2m+1}{4}\pi\right)}{\cosh\left(\frac{2m+1}{2}\pi\frac{K'}{K}\right)}\cos(2m+1)\theta. \tag{15}$$

Hence the equation for k reads, from Eq. (15),

$$\dot{k}=-\frac{\epsilon\omega\sqrt{1-k^2}}{k}\sum_{m=0}^{\infty}\frac{\cos\left(\frac{2m+1}{4}\pi\right)}{\cosh\left(\frac{2m+1}{2}\pi\frac{K'}{K}\right)}\times\cos(2m+1)\theta\ \sin\nu t, \tag{16}$$

where $K'\equiv K(k')$. As it follows from Eq. (16), the terms with phase oscillations of $\sin[(2m+1)\theta-\nu t]$ give the conditions for the first-order resonances:

$$(2m+1)\omega(k)=\nu,\quad m=0,1,2,\ldots. \tag{17}$$

Since $K(k)\geqslant K(0)$ and $K(0)=\pi/2$, Eq. (12) implies $\omega(k)\leqslant\omega(0)=1$. Therefore, there exists a sequence of special (boundary) frequencies $\{\nu^i\}=1,3,5,\ldots,2i+1,\ldots$ such that for $\nu^i<\nu<\nu^{i+1}$ only first-order resonances with winding numbers $2m+1$ greater than $2i+1$ are observed, as it can be seen from Eq. (17).

The typical resonance structure is demonstrated in Fig. 2. For the central point $p=q=0$ the unperturbed Hamiltonian takes value $\mathcal{H}_0=-2$ and therefore $k=0$. For a given value of ν the first-order resonance condition is satisfied for some value of k. The minimal possible value of m is denoted by $\bar{m}$. Therefore, the phase plane is divided into two regions, separated by the resonance with the smallest winding number $(2\bar{m}+1)$ for given ν [which will be called the lowest resonance (LR) below]. In the inner region only resonances of higher orders exist. For example, in the vicinity of the LR separatrix high-order resonances can take place due to the high-frequency perturbative term $\sin[(2m+1)\theta+\nu t]$ in Eq. (16). The outer region comprises resonances of all orders, starting with the first one. (According to this division the outer region includes the separating resonance as well.)

As the frequency ν approaches any of its boundary values $\{\bar{\nu}^m\}$ from below ($\bar{\nu}^m=3$ in the present case), the lowest resonance and its inner region shrink down to the central elliptic point and disappear when ν becames larger then $\bar{\nu}^m$ since the resonance condition (17) is no longer satisfied. The mechanism of disappearance of the LR represents a bifurcation of the connection of the LR hyperbolic and elliptic points with the central elliptic point. It is the so-called saddle-node bifurcation. Numerical experiments show that when $\nu\to\bar{\nu}^m$ the inner region collapses, while the period of motion grows to infinity, as it is expected from the fact that motion on the inner separatrix containing hyperbolic points has an infinite period. Indeed, when $k\to 0$ and $\omega(k)\to 1$ the phase $(2m+1)\theta-\nu t$ approaches zero for $\nu=\bar{\nu}^m$ as well and the period of phase oscillations goes to infinity.

For Eq. (17) we can see how the chain of elliptic and hyperbolic points corresponding to the resonance $\bar{m}$ approaches the origin in phase space where $k=0$, as ν approaches $\bar{\nu}^m$. For this purpose the expansion in k of the complete elliptic integral $K(k)\approx(\pi/2)[1+k^2/4+\cdots]$ is used [13]. The resonance condition (17) reads

$$(2m+1)\omega(k)\approx(2m+1)\left[\omega(0)-\frac{k^2}{4}\right]=\nu. \tag{18}$$

If the deviation from the boundary frequency $\bar{\nu}^m$ is $\delta=(\bar{\nu}^m-\nu)/\bar{\nu}^m$, the value of k where the resonance condition (18) is satisfied is

$$\bar{k}_m=2\sqrt{\delta}. \tag{19}$$

This is the value of k where the chain of elliptic and hyperbolic points with winding numbers $2\bar{m}+1$ is found. As $\delta\to 0$ also $k\to 0$, thus the chain approaches the origin and the distance between the various points in phase space decreases as $\delta^{1/2}$. This fact agrees with general theory of bifurcation of equilibrium points [14]. From Fig. 2(c) one can see the island chains of the resonances with $m=2$ and 3.

The case $\bar{\nu}^{m=0}=1$ stands separately in the sense that connection occurs between the LR hyperbolic point and the central elliptic point. It is shown in Fig. 3 that these points disappear when the bifurcation takes place and the LR elliptic point survives. At $\nu\geqslant 1$ this point becomes the central elliptic one with $k=0$. Thus the result (19) is valid for $\bar{\nu}^m=1$ as well. This reflects the fact that in the absence of additional symmetry (like rotation by $2\pi/3$ in the previous case) the LR hyperbolic point approaches the central elliptic point (the point of the bifurcation) faster than the LR elliptic one. Equation (19) describes the bifurcate reconstruction of the phase space for any boundary frequencies $\bar{\nu}^m$ and for ϵ sufficiently small for the isolated resonance approximation to hold.

III. SEPARATRIX MAP

Until now the dynamics in the first Brillouin zone, i.e., in the cell $-\pi\leqslant p,q\leqslant\pi$, was studied. In extended picture all phase space is covered by a separatrix mesh, as shown in Fig. 1. The phase space is symmetric under the translations (6) and (7) for $\epsilon=0$, as was mentioned above. As a result of the action of the perturbation ϵV, the separatrix mesh acquires a finite width and chaotic motion takes place inside

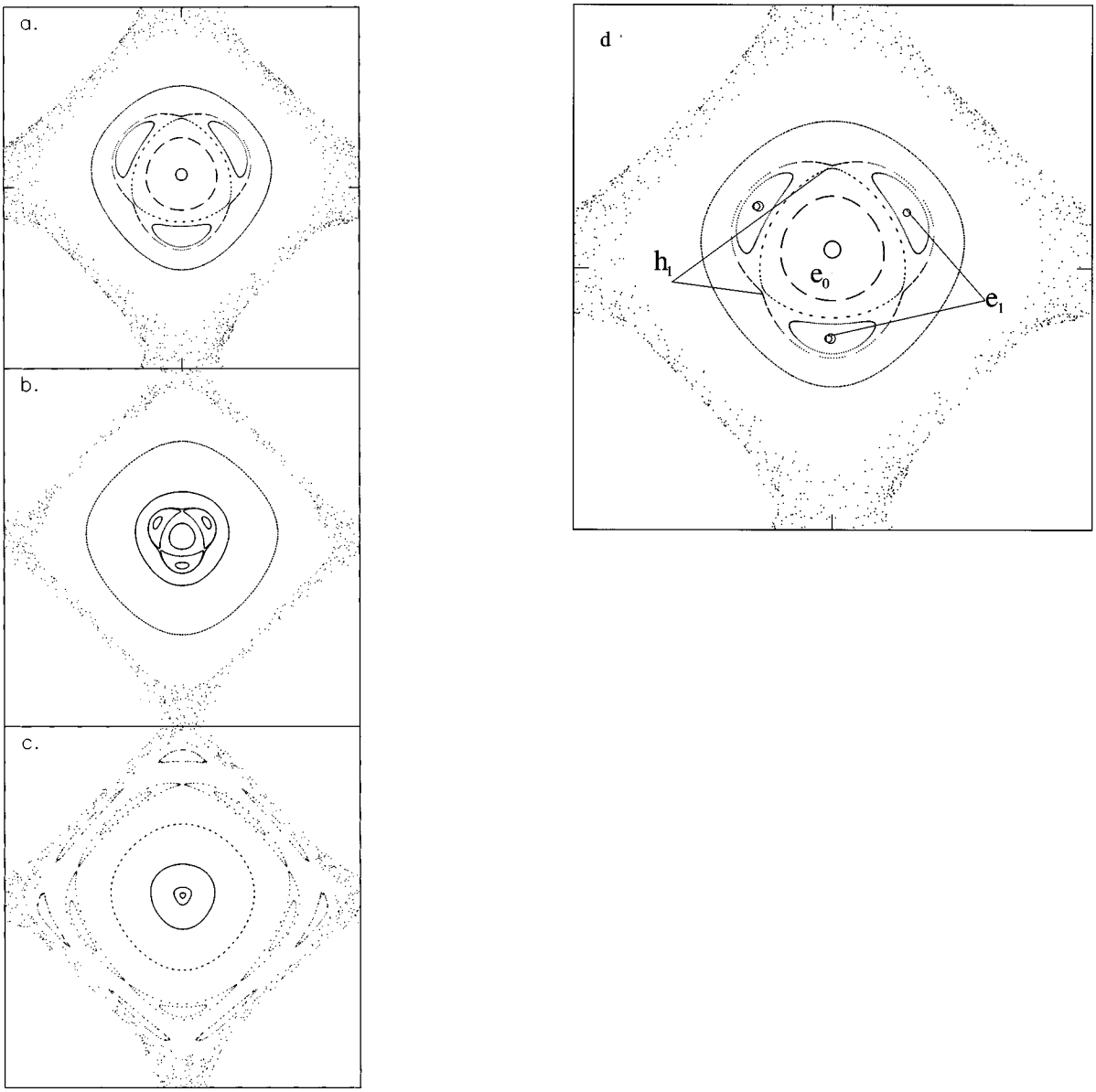

FIG. 2. Bifurcation of the lowest resonance for $\epsilon=0.5$ and $\nu<\nu_{crit}$ with $\nu_{crit}=3$, which is a typical case. The values of the parameters are (a) $\nu=2.60$, (b) $\nu=2.90$, and (c) $\nu=2.99$. (d) Zoom of (a). e_0 denotes the central elliptic point, while e_1 and h_1 are elliptic and hyperbolic points of the LR, respectively.

this region [6,10–12,15]. This leads to unlimited diffusion in the extended phase space along the separatrix mesh [6]. In order to describe the motion in a stochastic layer it is convenient to introduce a separatrix map [4,10]. This map is usually written for an energy-time canonical pair (w,τ), where w denotes an energy of the unperturbed system with the Hamiltonian $\mathcal{H}_0$ and τ determines a phase of the perturbative field $\epsilon V(q)\sin\nu(t+\tau)$. Therefore, to construct the map one needs to calculate the energy change $\Delta w\equiv\Delta\mathcal{H}_0=\overline{w}-w$ over a time interval between two successive passages in the vicinity of two consequently connected hyperbolic points, for example, i and f in Fig. 1 at times $\overline{\tau}$ and τ. This time interval $\Delta\tau=\overline{\tau}-\tau$ is equal to one-quarter of the period:

$$\Delta\tau=\frac{1}{4}T=\frac{\pi}{2\omega}=K(k). \tag{20}$$

Hence the change of energy determined by the perturbation is

$$\Delta w=\int_{-\Delta\tau/2}^{\Delta\tau/2}\dot{\mathcal{H}}_0 dt=\epsilon\int_{-\Delta\tau/2}^{\Delta\tau/2}\frac{\partial V}{\partial q}\dot{q}\ dt. \tag{21}$$

Expression (21) is a particular case of the Melnikov-Arnold integral [10–12,15]. Now the integral on trajectories close to the separatrix will be approximated by its value on the separatrix where the period is infinite. The velocity $\dot{q}$ taken on the separatrix of the unperturbed motion is obtained from Eq. (9). In the case when $\mathcal{H}_0=0$ it reads

$$t=\int^{x}\frac{dx'}{1-x'^2}, \tag{22}$$

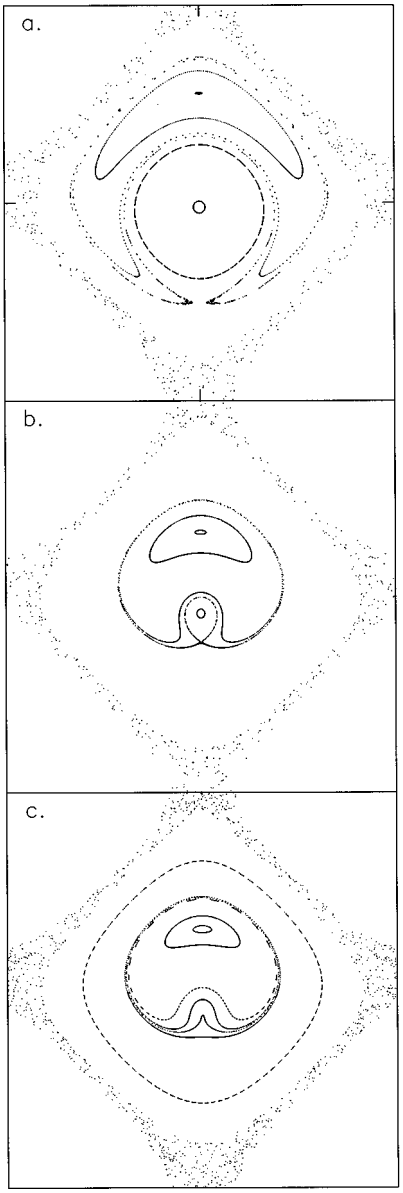

FIG. 3. Same as Fig. 2 for $\nu_{crit}=1$. The values of the parameters are $\epsilon=0.05$ and (a) $\nu=0.70$, (b) $\nu=0.90$, and (c) $\nu=0.92$.

where the limit of $x=1$ must be avoided. Calculating this integral, we obtain for the time and coordinate $t=-\frac{1}{2}\ln[(1-\cos q)/(1+\cos q)]$ and $\cos q=(1-e^{-2t})/(1+e^{-2t})$. Therefore, on the separatrix $\dot{q}=\sin p=\sqrt{1-\cos^2 p}=\sqrt{1-\cos^2 q}=1/\cosh t$. The limits of integration in Eq. (21) are moved to infinity. After substitution of the explicit expressions for $V(q,t)$ from Eq. (5) and $\dot{q}$, expression (21) assumes the form

$$\Delta w=\epsilon\int_{-\Delta\tau}^{\Delta\tau}\frac{\sin\nu(t+\tau)}{\cosh t}dt=\epsilon\int_{-\infty}^{\infty}\frac{\sin\nu(t+\tau)}{\cosh t}dt$$

$$=\frac{\epsilon\pi}{\cosh\dfrac{\pi\nu}{2}}\sin\nu\tau. \tag{23}$$

In the vicinity of the separatrix $\Delta\tau$ is large [see also Eq. (24) below] and the integrand decays exponentially with time; therefore, the error introduced replacing $\Delta\tau$ by ∞ in the integral is exponentially small in $\Delta\tau$.

On the separatrix $k\to 1$ and $k'\to 0$, hence

$$\Delta\tau=K(k)\approx\ln\frac{4}{k'}=\ln\frac{8}{|w|} \tag{24}$$

and the period goes to infinity. These two conditions are the standard approximations used to describe the motion in the small vicinity near the separatrix [10–12,15].

Thus, summarizing the above formulas, one gets the separatrix map

$$\bar{w}=w+\Lambda\sin\nu\tau,$$

$$\bar{\tau}=\tau+\ln\frac{8}{|\bar{w}|}. \tag{25}$$

Here $\Lambda=\epsilon\pi/\cosh(\pi\nu/2)$. It can be generated by the Hamiltonian

$$H_{sep}=H_0(w)+\frac{\Lambda}{\nu}\cos\nu\tau\sum_{n=-\infty}^{\infty}\delta(t-n) \tag{26}$$

and $\partial H_0(w)/\partial w=\ln(8/|w|)$.

IV. ACCELERATION MODE

To proceed, we will consider an acceleration mode dynamics. First, however, it is worthwhile to describe how the map (25) governs the particle motion inside the separatrix chaotic mesh. The separatrix mesh determines the direction of motion between hyperbolic points. For $w<0$ the direction of the motion is counterclockwise, whereas for $w>0$ the motion is in the clockwise direction (see Fig. 1), as can be seen by linearization around the hyperbolic fixed points. Note that w changes sign at each separatrix line. Therefore, the trajectory either penetrates a different cell or stays in the same cell. This is determined by the sign change of w after one iteration of the map (25). Thus, given an initial condition w_0 at some time τ_0 it is possible to determine the position of the trajectory at $\bar{\tau}=\tau_0+T(w_0)$. A ballistic trajectory that crosses the separatrix at each iteration of the map (25) and a w that changes its sign at every step (see Figs. 1 and 4) can be found. An acceleration mode of the system (5) and (3) is, for example, a periodic orbit of period 2 of Eq. (25). Such an acceleration mode appears when

$$\tau=\tau_0\equiv\pm\frac{\pi}{2\nu},\quad w=w_0\equiv\mp 8e^{-\pi J/\nu},\quad \Lambda=\Lambda_0\equiv 2|w_0|, \tag{27}$$

where J is an odd integer. The points (w_0,τ_0) are parabolic points [16,17]. When any chaotic trajectory reaches the small vicinity of these points it can be captured for some time by an acceleration mode and will contribute strongly to the diffusion.

To evaluate the maximal length of such a ballistic trajectory, defined by Eq. (27), one can consider dynamics in the small vicinity of the point (τ_0,w_0). As it is seen from Fig. 5(a) an escape from the parabolic point occurs only in one

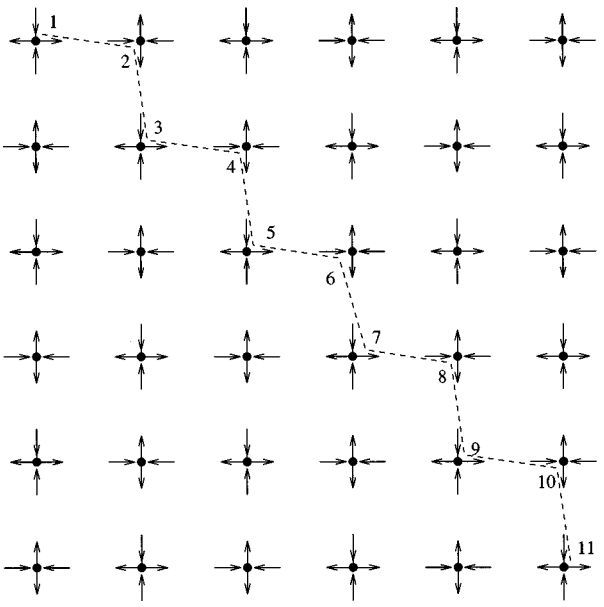

FIG. 4. Ballistic trajectory in (q,p) space. The coordinates of the separatrix mesh are rotated by $\pi/4$ with respect to Fig. 1.

direction and one-dimensional motion in the τ direction can be considered. For definiteness the lower sign in Eq. (27) will be taken in what follows. We turn now to estimate the number of steps n_1 required to escape to a distance of order 1 from the parabolic point. Defining a phase $\phi=\nu\tau=\phi_0+\Delta=\nu\tau_0+\Delta$, where $|\Delta|\ll 1$ is a small deviation from the parabolic point, we obtain from Eqs. (25) and (27) that $\bar{w}=w_0+\Lambda_0\sin(\phi_0+\Delta)\approx -w_0+\Lambda_0(\Delta^2/2)$ and

$$\bar{\phi}=\phi_0+\Delta+\nu\ln\frac{8}{|\bar{w}|}\approx\phi_0+\Delta+J\pi+\nu\Delta^2. \tag{28}$$

Then it is natural to define $\bar{\phi}=\bar{\phi}_0+\bar{\Delta}$, where $\bar{\phi}_0=\phi_0+J\pi$. The resulting map for Δ is $\bar{\Delta}=\Delta+\nu\Delta^2$, or rewriting it for arbitrary step $n=0,1,2,\ldots$

$$\Delta_1=\Delta+\nu\Delta^2,\quad \Delta_2=\Delta_1+\nu{\Delta_1}^2=\Delta+2\nu\Delta^2,\ldots,$$

$$\Delta_n=\Delta+n\nu\Delta^2,\ldots. \tag{29}$$

Choose now a value $n^*=[1/\nu\Delta]+1$, where $[\ ]$ is the integer part; then $\Delta_{n^*-1}<2\Delta<\Delta_{n^*}$. This will give an overestimate of n_1 by a number of order $\nu\Delta$. Defining $2\Delta=\tilde{\Delta}$, we can define again $\tilde{n}^*=[1/\nu\tilde{\Delta}]+1$ so that $\tilde{\Delta}_{\tilde{n}^*-1}<2\tilde{\Delta}<\tilde{\Delta}_{\tilde{n}^*}$. Repeating this procedure until $\Delta_{n_1}=1$, one obtains that for $\Delta\ll 1$,

$$n_1=n^*+\tilde{n}^*+\cdots=\frac{1}{\nu\Delta}\left(1+\frac{1}{2}+\frac{1}{4}+\cdots\right)\approx\frac{2}{\nu\Delta}. \tag{30}$$

Numerical calculations of the integrated probability distribution of the free path lengths for various values of the parameters ν and J show that the maximal escape time agrees with the estimation of n_1 found from Eq. (30) for $0<\Delta\leqslant 0.01$.

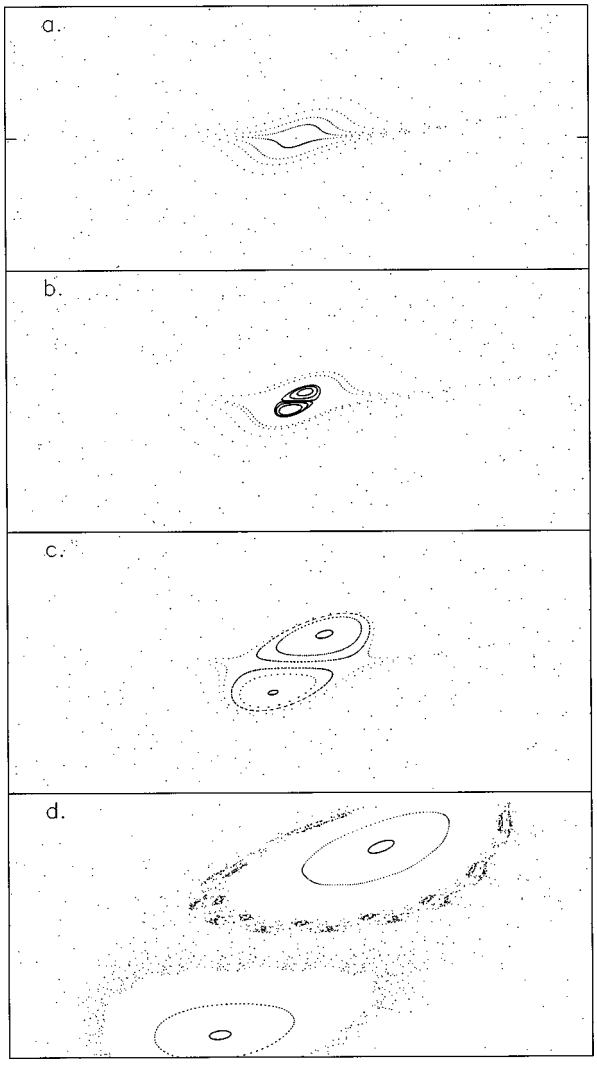

FIG. 5. Bifurcation of the acceleration mode periodic point for $J=3$ and (a) $\delta=0.0$, (b) $\delta=1.0\times10^{-6}$, and (c) $\delta=1.0\times10^{-5}$, and (d) $\delta=1.0\times10^{-4}$.

For negative Δ this estimate fails since the terms alternate in sign. In this case the terms of order Δ^3 should be taken into account.

When $\Lambda=\Lambda_0(1+\delta)$ with $0<\delta\ll 1$ a saddle-node bifurcation takes place and the parabolic point disintegrates into two elliptic and two hyperbolic points. The process of confluence of these points as $\delta\to 0$ is shown in Figs. 5(a)–5(d). A mechanism of such a bifurcation can be understood from the following analysis of determining of these four stationary points. Iterating the separatrix map twice, one obtains from Eq. (25)

$$w_{n+2}=w_n+\Lambda\sin\phi_n+\Lambda\sin\left(\phi_n+\nu\ln\frac{8}{|w_n+\Lambda\sin\phi_n|}\right),$$

$$\phi_{n+2}=\phi_n+\nu\ln\frac{8}{|w_n+\Lambda\sin\phi_n|}+\nu\ln\frac{8}{|w_{n+2}|}. \tag{31}$$

The conditions on the stationary points $w_{n+2}=w_n\equiv w$ and $\phi_{n+2}=\phi_n\equiv\phi$ lead to

$$\sin\left(\phi+\frac{\nu}{2}\ln\frac{8}{|w+\Lambda\sin\phi|}\right)\cos\left(\frac{\nu}{2}\ln\frac{8}{|w+\Lambda\sin\phi|}\right)=0, \tag{32}$$

$$-\ln\frac{8}{|w+\Lambda\sin\phi|}=\ln\frac{8}{|w|}\pm\frac{2\pi n}{\nu}. \tag{33}$$

Consequently, one obtains

$$\frac{\nu}{2}\ln\frac{8}{|w+\Lambda\sin\phi|}=\pm J\frac{\pi}{2},\quad J=2n+1 \tag{34}$$

or

$$\phi+\frac{\nu}{2}\ln\frac{8}{|w+\Lambda\sin\phi|}=0,\pm n\pi, \tag{35}$$

where J is the same as in Eq. (27), while n is an integer. We will choose solutions that have physical meaning such that $|w|<1$, $|\phi-\phi_0|\ll\phi_0$. Therefore, it follows from Eq. (34) that $\ln(8/|w+\Lambda\sin\phi|)=-J\pi/\nu$ and from Eq. (33) one obtains that the solutions for w are

$$|w|=8e^{-J\pi/\nu}=|w_0|. \tag{36}$$

We require (as for $\delta=0$) that at the fixed point w just changes sign between consecutive iterations leading to $|w+\Lambda\sin\phi|=|w|$ and, consequently, the solution for the phase is determined from

$$\cos\Delta\phi=\frac{1}{1+\delta}, \tag{37}$$

where $\Delta\phi=\phi-\phi_0$ and ϕ_0 is the value for $\delta=0$. One can check by the linearization of Eq. (31) that these solutions correspond to the hyperbolic points with $\Delta\phi\approx\pm\sqrt{2\delta}$. The distance between them is of order $2\sqrt{2\delta}$, which corresponds to expression (19) for the bifurcation analysis.

The other two points that are elliptic can be found from Eq. (35), which can be rewritten as $2\phi+\nu\ln(8/|w+\Lambda\sin\phi|)=0\pm2\pi n$. Therefore, with the help of Eq. (33) one obtains that $|w|=8e^{-2(\phi+m\pi)/\nu}$. Taking $\phi=\phi_0+\Delta\phi=\pi/2+\Delta\phi$ and $w_0=-8e^{-J\pi/\nu}$ [see Eq. (27)], we obtain for the first elliptic point

$$w_1=-|w_0|e^{-2\Delta\phi/\nu},\quad J=2m+1. \tag{38}$$

Taking $\phi=-\pi/2+\Delta\phi$ and $w_0=+8e^{-J\pi/\nu}$, we obtain the second solution where $w_2=-w_1$. It follows from Eq. (33) that $\Delta\phi$ satisfies

$$(1+\delta)\cos(\Delta\phi)=\cosh\left(\frac{2\Delta\phi}{\nu}\right). \tag{39}$$

Numerical computations with different distributions of initial conditions and various parameters $\{\delta,\nu,J\}$ show that both normal diffusion and acceleration take place. A typical random walk with normal diffusion $\langle p^2+q^2\rangle\sim Dt$ takes place when the perturbation parameter $\Lambda=\Lambda_0(1+\delta)<\Lambda_0$, i.e., $\delta<0$. The parabolic point representing the acceleration mode disappears and no elliptic islands are found.

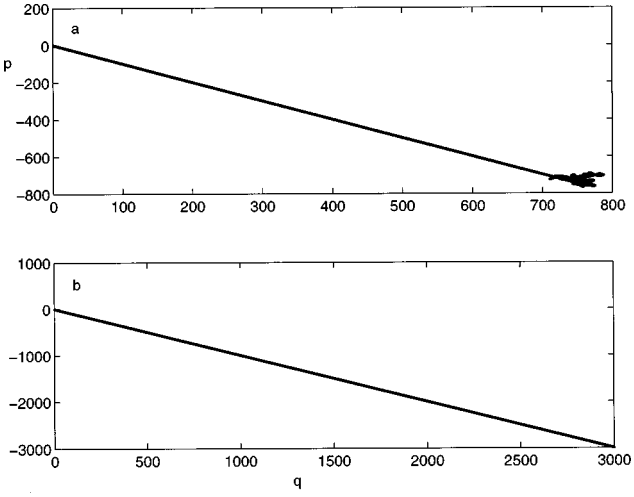

FIG. 6. Ballistic flights for $\nu=1$, $J=1$, and (a) $\delta=10^{-6}$ and (b) $\delta=10^{-5}$.

Numerical simulations show that for $\delta>0$ there is ballistic motion for a very long time. The motion follows roughly the one that was schematically plotted in Fig. 4. Consequently trajectories in phase space are approximately straight lines as demonstrated in Fig. 6. This results in ballistic motion where $D(t)\sim t$ for a finite interval of time that increases with δ, as shown in Fig. 7. For $\delta=10^{-6}$ this interval is $t\leqslant1500$, as seen in Fig. 7(a), while for $\delta=10^{-5}$ it is too long to be observed in the simulation. The reason is that as δ increases the elliptic island that is accelerated with what was the accelerator mode for $\delta=0$ is larger and therefore the sticking probability to it is larger. For a longer time scale where ordinary diffusion is observed $D(t)=\text{const}$ [Fig. 7(a)]. This mechanism where stickiness leads to acceleration and anomalous diffusion was discussed for other systems [15,16,18].

V. CONCLUSIONS

In this paper the regular and chaotic dynamics of the nonlinear system with a periodic phase space has been investi-

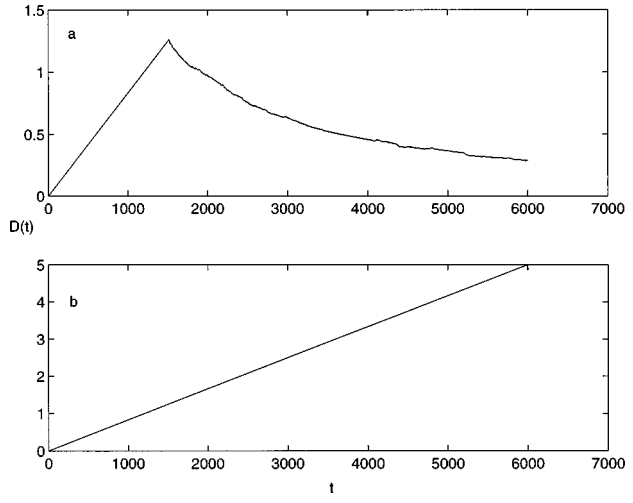

FIG. 7. Diffusion coefficient vs time t. Averaging is carried out over 300 initial conditions with $\phi=\nu\tau$ uniformly distributed in the interval $[-\pi/2,\pi/2]$. The values of the parameters are $\nu=1$, $J=1$, and (a) $\delta=10^{-6}$ and (b) $\delta=10^{-5}$.

gated. This periodicity is due to the symmetry of the Fermi surface, which leads to the division of phase space into $2\pi\times 2\pi$ cells separated by the separatrix mesh. The centers of the cells are elliptic points with $\mathcal{H}_0=-2$ for the motion of electrons and $\mathcal{H}_0=2$ for the motion of holes. The vertices of the mesh are hyperbolic points (see Fig. 1). Chaotic behavior and other interesting phenomena resulting from nonlinearity are induced by the external fields. The main feature of this dynamics is that there are nonlinear resonances between internal cyclotron motion and the alternating electric field. The nature of these resonances is described for both motion around of a central elliptic point and motion in the vicinity of separatrix, separating motion between clockwise and counterclockwise directions. The second important feature of this dynamics is that the phase space is periodic in both q and p directions. The motion in the vicinity of stationary points of the mesh (elliptic and hyperbolic) was considered in detail and the implications for the global dynamics were studied.

The bifurcate reconstruction of the phase space studied here apparently represents a particular case of reconstruction of the phase space for systems with some symmetry with respect to rotations around a central point, which is perturbed by a one-frequency perturbation. The main result is that as the driving frequency ν increases, the low-order resonances shrink to the center of the cell and disappear. The winding number $2\overline{m}+1$ for the lowest resonance is approximately $\nu=\widetilde{\nu}/\Omega$, where $\widetilde{\nu}$ is the driving frequency and Ω is the cyclotron frequency. Its effects can be studied by cyclotron resonance experiments in two-dimensional electronic systems in the case of microwave frequencies of the alternating field ($\nu\approx 1$) and the magnitude of the magnetic field H for which the condition $\omega_c\tau_r>1$ is satisfied, where τ_r is the relaxation time. When a magnetic flux of H is large enough, quantum effects that were not considered here become important.

The motion in the chaotic mesh that connects the vertices of the cells was studied in the framework of the separatrix map. A specific acceleration mode was identified and its bifurcations, resulting from the variation of the parameters, were studied in detail. These result in a transition between diffusion and acceleration. At the value of the parameter where the transition takes place the transport is dominated by a parabolic fixed point. In this case transport is dominated by trajectories that stick for a long time to this point that is accelerated. A change in parameters may lead to an accelerated elliptic islands. Trajectories that are trapped in these islands are accelerated. Their presence also enhances the diffusion of trajectories that lie in the chaotic mesh, since these stick for a long time to the accelerated islands. These results should manifest themselves in the conductivity of the relevant systems, as can be verified with the help of the standard methods [4,5,7]. The details of these will be presented elsewhere [19].

The materials that are most relevant for experimental realization of the cyclotron resonance effects that were studied in the present paper are the two-dimensional electron gas embedded in lateral superlattices fabricated on GaAs heterostructures [20] and organic metals [21,22]. Classical calculations in the chaotic regime were used to explain the microwave photoconductivity for GaAs heterostructures [23]. The experimental and theoretical explorations of the organic metals focused so far on their Fermi surfaces that are quasi-two-dimensional. The topologies of these surfaces are studied by a variety of strong magnetic field [21] as well as cyclotron resonance [22,24] techniques. The tight-binding model (2) is used for these investigations [25]. For the organic metals the skin depth is larger than the size of the small crystals used in resonant microwave cavity experiments [25]. These experiments are not in the Azbel'-Kaner regime [22,25] and a different nonlinear theory of the nature of the one presented here is required.

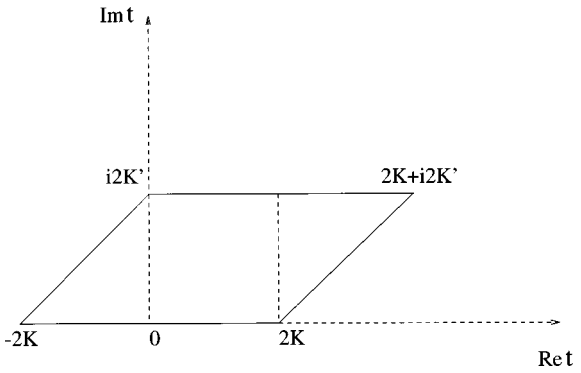

FIG. 8. Contour of integration used in the Appendix.

If the motion can be modeled in the framework of classical dynamics, the description by the separatrix map (25) is quite general. It can be used in the studies of electronic dynamics in magnetic fields where anomalous diffusion of the guiding center takes place [26], anomalous diffusion in Josephson junctions [27], as well as for other intermittent chaotic systems [28]. The crucial point for these is the escape from the acceleration mode that is modeled by Eqs. (28)–(30).

ACKNOWLEDGMENTS

A.I. would like to thank V. Valkov for helpful and stimulating discussions at the initial stage of the work. This research was supported by the Ministry of Absorption of Israel, by the Minerva Center for Nonlinear Physics of Complex Systems, by the U.S.–Israel Binational Science Foundation, and by the Technion V.P.R. Fund – E. and J. Bishop Research Fund.

APPENDIX: FOURIER COEFFICIENTS OF sin$p$

The function sin$p$ given by Eq. (13) is expanded in Fourier components of $\theta=\omega t$ for $\epsilon=0$. We have to calculate the expansion coefficients A_n of

$$\sin p=\sum_{n=-\infty}^{\infty} A_n \exp(in\theta). \tag{A1}$$

It is convenient to define

$$B_n=\frac{\pi A_n}{R}=\int_{-\pi}^{\pi}\frac{\mathrm{cn}\,\dfrac{\theta}{\omega}}{\mathrm{dn}^{\,2}\dfrac{\theta}{\omega}+k'}e^{-in\theta}d\theta, \tag{A2}$$

where $R=k\sqrt{k'(k'+1)}$. To evaluate the integral, we will consider a closed path along a parallelogram in the complex $t=\theta/\omega$ plane (see Fig. 8), with edges separated by the primitive periods of the elliptic cosine, namely, $4K(k)$ and $2K(k)+i2K'(k)=2K(k)(1+\gamma)$, with $\gamma=iK'/K$. The integration along the path is the sum of the integrals along each side of the parallelogram:

$$\oint_C = \int_{\pi}^{2\pi+\gamma\pi} + \int_{2\pi+\gamma\pi}^{\gamma\pi} + \int_{\gamma\pi}^{-\pi} + \int_{-\pi}^{\pi} \equiv \int_1 + \int_2 + \int_3 + \int_4. \tag{A3}$$

We obtain from the periodicity of the integrand that

$$\int_1 + \int_3 = 0; \quad \int_2 + \int_4 = (1-e^{-in\pi(1+\gamma)}) \int_4. \tag{A4}$$

Hence

$$B_n = \frac{1}{1-e^{-in\pi(1+\gamma)}} \oint_C \frac{\mathrm{cn}\,\dfrac{\theta}{\omega}}{\mathrm{dn}^{\,2}\dfrac{\theta}{\omega}+k'} e^{-in\theta} d\theta. \tag{A5}$$

The last integral in Eq. (A5) is carried out by the residue method. Zeros θ_ν of the denominator inside the contour are

$$\theta_1 = \frac{-\pi}{4} + \frac{\gamma\pi}{2}, \quad \theta_2 = \frac{\pi}{4} + \frac{\gamma\pi}{2}, \quad \theta_3 = \frac{3\pi}{4} + \frac{\gamma\pi}{2},$$

$$\theta_4 = \frac{5\pi}{4} + \frac{\gamma\pi}{2} \tag{A6}$$

and the residues are

$$\operatorname*{res}_{\theta=\theta_\nu} = -\frac{\pi}{2K(k)} \frac{e^{-in\theta_\nu}}{2k^2\,\mathrm{sn}\,\dfrac{\theta_\nu}{\omega}\,\mathrm{dn}\,\dfrac{\theta_\nu}{\omega}}.$$

Finally, we obtain for the expansion coefficients A_n

$$A_{2l}=0, \quad A_{2l+1} = \frac{2\omega\cos\dfrac{2l+1}{4}\pi}{\cosh(2l+1)\dfrac{\pi K'}{2K}}, \tag{A7}$$

leading to Eq. (15).

[1] A. P. Gracknell and K. C. Wong, *The Fermi Surface* (Clarendon, Oxford, 1973).
[2] I. M. Lifshitz, M. Ya. Azbel, and M. I. Kaganov, *Electron Theory of Metals* (Consultants Bureau, New York, 1973).
[3] J. M. Luttinger, Phys. Rev. **84**, 814 (1951).
[4] T. Geisel, J. Wagnehuber, P. Niebauer, and G. Obermair, Phys. Rev. Lett. **64**, 1581 (1990); J. Wagenhuber, T. Geisel, P. Niebauer, and G. Obermair, Phys. Rev. B **45**, 4372 (1992); R. Fleischmann, T. Geisel, R. Ketzmerick, and G. Petschel, Physica D **86**, 171 (1995), and references therein.
[5] R. Fleischmann, T. Geisel, and R. Ketzmerick, Phys. Rev. Lett. **68**, 1367 (1992).
[6] G. M. Zaslavsky, M. Yu. Zakharov, R. Z. Sagdeev, D. A. Usikov, and A. A. Chernikov, Zh. Éksp. Teor. Fiz. **91**, 500 (1986) [Sov. Phys. JETP **64**, 294 (1986)].
[7] T. Geisel, A. Zacherl, and G. Radons, Phys. Rev. Lett. **59**, 2503 (1987); Z. Phys. B **71**, 117 (1988).
[8] C. Kittel, *Introduction to Solid State Physics* (Wiley, New York, 1971).
[9] A. P. Prudnikov, Yu. A. Brychkov, and O. I. Marichiv, *Integrals and Series* (Gordon and Breach, New York, 1986).
[10] B. V. Chirikov, Phys. Rep. **52**, 265 (1979).
[11] A. J. Lichtenberg and M. A. Lieberman, *Regular and Stochastic Motion* (Springer-Verlag, New York, 1983).
[12] G. M. Zaslavsky, *Chaos in Dynamic Systems* (Harwood Academic, New York, 1985).
[13] E. Janke, F. Emde, and F. Lösh, *Tables of Higher Functions* (Teubner Verlagsgesellschaft, Stuttgart, 1960).
[14] V. I. Arnol'd, *Catastrophe Theory* (Springer, Berlin, 1986).
[15] G. M. Zaslavsky, Chaos **4**, 589 (1994).
[16] G. M. Zaslavsky, M. Edelman, and B. Niyazov, Chaos **7**, 159 (1997), and references therein.
[17] V. Melnikov, in *Transport, Chaos, and Plasma Physics*, edited by S. Benkadda, F. Doveil, and Y. Elskens (World Scientific, Singapore, 1995), p. 142.
[18] G. M. Zaslavsky, Physica D **76**, 110 (1994); J. D. Meiss, Phys. Rev. A **34**, 2375 (1986); R. S. MacKay, Physica D **7**, 283 (1983).
[19] A. Iomin and S. Fishman (unpublished).
[20] For a review see W. Hansen, U. Merkt, and J. P. Kotthaus, in *Nanostructured Systems*, edited by M. Reed, Semiconductors and Semimetals Vol. 35 (Academic, San Diego, 1992), p. 279.
[21] J. Wosnitza, *Fermi Surfaces of Low-Dimensional Organic Metals and Superconductors* (Springer, Berlin, 1996).
[22] S. Hill, Phys. Rev. B **55**, 4931 (1997), and references therein.
[23] E. Vasiliadou, *et al.*, Phys. Rev. B **52**, R8658 (1995).
[24] J. Singleton *et al.*, Phys. Rev. Lett. **68**, 2500 (1992); J. Singleton *et al.*, Physica B **184**, 470 (1993).
[25] S. J. Blundel, A. Ardavan, and J. Singleton, Phys. Rev. B **55**, R6129 (1997).
[26] G. Petschel and T. Geisel, Phys. Rev. A **44**, 7959 (1991).
[27] T. Geisel, J. Nierwetberg, and A. Zacherl, Phys. Rev. Lett. **54**, 616 (1985).
[28] T. Geisel and S. Thomae, Phys. Rev. Lett. **52**, 1936 (1984); I. Procaccia and H. Schuster, Phys. Rev. A **28**, 1210 (1983); P. Manneville, J. Phys. (Paris) **41**, 1235 (1980).